Using bimodal MRI/fluorescence imaging to identify host angiogenic response to implants

Alexandra Berdichevski[a], Haneen Simaan Yameen[a], Hagit Dafni[b], Michal Neeman[c], and Dror Seliktar[a,1]

[a]Faculty of Biomedical Engineering, Technion – Israel Institute of Technology, Haifa 32000, Israel; and Departments of [b]Veterinary Resources and [c]Biological Regulation, Weizmann Institute of Science, Rehovot 76100, Israel

Edited by Robert Langer, Massachusetts Institute of Technology, Cambridge, MA, and approved March 10, 2015 (received for review February 18, 2015)

Therapies that promote angiogenesis have been successfully applied using various combinations of proangiogenic factors together with a biodegradable delivery vehicle. In this study we used bimodal noninvasive monitoring to show that the host response to a proangiogenic biomaterial can be drastically affected by the mode of implantation and the surface area-to-volume ratio of the implant material. Fluorescence/MRI probes were covalently conjugated to VEGF-bearing biodegradable PEG-fibrinogen hydrogel implants and used to document the in vivo degradation and liberation of bioactive constituents in an s.c. rat implantation model. The hydrogel biodegradation and angiogenic host response with three types of VEGF-bearing implant configurations were compared: preformed cylindrical plugs, preformed injectable microbeads, and hydrogel precursor, injected and polymerized in situ. Although all three were made with identical amounts of precursor constituents, the MRI data revealed that in situ polymerized hydrogels were fully degraded within 2 wk; microbead degradation was more moderate, and plugs degraded significantly more slowly than the other configurations. The presence of hydrogel degradation products containing the fluorescent label in the surrounding tissues revealed a distinct biphasic release profile for each type of implant configuration. The purported in vivo VEGF release profile from the microbeads resulted in highly vascularized s.c. tissue containing up to 16-fold more capillaries in comparison with controls. These findings demonstrate that the configuration of an implant can play an important role not only in the degradation and resorption properties of the materials, but also in consequent host angiogenic response.

biomaterial scaffold | angiogenesis | hydrogel | contrast agents | tissue regeneration

With progress in the field of regenerative medicine relying more on approaches that deliver cells and/or bioactive factors using minimally invasive procedures, functional donor-to-host integration remains a critical challenge. In this context, biodegradable hydrogel scaffolds provide certain advantages, such as excellent tissue compatibility, temporary protection from host inflammation, and controlled resorption based on cell-mediated degradation (1). Effective transport properties to and within an implanted hydrogel are critical in the design of cell-seeded scaffolds, where the delivery of nutrients and removal of waste products from regions deep within the implant can severely limit the use of a patch for only the smallest of grafts (i.e., <0.5 mm) (2–4). Therefore, a great deal of research in the field of regenerative medicine has been devoted to ameliorate the survival of the cells and tissues with implants that use proangiogenic factors.

One strategy is to enhance the localized formation of vascularized networks to improve the perfusion of oxygen and nutrients to the intended region in the body (2, 4, 5). This process is regulated by a number of different growth factors that stimulate a complex angiogenic response based on unique temporal and spatial distributions (6–8). VEGF is one such agonist that is known to be essential and specific for angiogenesis (8–10). Although VEGF has been used exogenously to promote in vivo angiogenesis, superior results were obtained when the factor was protected, localized, and temporally controlled at the site of implantation (7, 10, 11). The hypothesis underlying this study is that degradation and resorption characteristics of the implant may be influenced by its surface area-to-volume ratio and mode of implantation, and hence the release properties of the proangiogenic factors within the implant site can be optimized accordingly (12–15). As a case in point, an injectable strategy whereby the hydrogel precursor solution is injected and cross-linked in situ allows an even and contiguous dispersion of the hydrogel within the injury interstitial space for better host integration. However, the less controllable cross-linking efficiency of the injectable hydrogel, compared with a large preformed patch construct, can provide a more rapid degradation profile as well as faster release of proangiogenic factors—irrespective of its higher surface area-to-volume ratio. Another approach is using injectable microbeads, which combine the advantages of high surface area-to-volume ratio and more controlled cross-linking efficiency. The use of implant configuration as a basis for producing more potent constructs for tissue engineering and induction of angiogenesis have been inadvertently underestimated and still remain poorly studied for lack of good experimental tools that can continuously and noninvasively monitor the fate of the implants in vivo.

Various invasive techniques have been described for documenting implant resorption in vivo; however, these techniques do not provide detailed information about the in situ integration process and require destructive analysis of postmortem sections (13, 16–18). With the optimization of a hydrogel scaffold requiring more information of the transient steps of integration, techniques to continuously monitor the degradation of a scaffold using fluorescence labeling have been described (15, 19, 20). However, in vivo fluorescence monitoring of biomaterials often results in a diffuse signal that does not allow for accurately determining the implant volume or its exact anatomical placement. Rather, fluorescence provides important information about the

Significance

The current investigation applies a bimodal imaging technique to uncover a newfound appreciation for the mode of implantation as it relates to the vascularization events associated with proangiogenic therapy. We apply our ability to noninvasively track the precise in vivo fate of an implanted proangiogenic vehicle to show that the subsequent vascular network formation is related directly to the mode of implantation vis-à-vis the biodegradation and bioresorption profiles. The findings in this study uncover important insights about angiogenesis, noninvasive in vivo monitoring, and biomaterials design that should be very beneficial to a wide scientific audience in the regenerative medicine field.

Author contributions: A.B., H.S.Y., H.D., M.N., and D.S. designed research, performed research, contributed new reagents/analytic tools, analyzed data, and wrote the paper.

The authors declare no conflict of interest.

This article is a PNAS Direct Submission.

[1]To whom correspondence should be addressed. Email: dror@bm.technion.ac.il.

This article contains supporting information online at www.pnas.org/lookup/suppl/doi:10.1073/pnas.1502232112/-/DCSupplemental.

distribution and bioresorption of the labeled degradation products that are released from the implant. In contrast, MRI has the ability to pinpoint the exact in vivo anatomical location, including its 3D shape and volume. In recent years, MRI has become one of the most universal techniques aimed at visualizing detailed internal structures in the body. The use of contrast agents for MRI provides comparable spatial resolution with far better contrast resolution than CT imaging (21, 22). Furthermore, the use of both MRI and fluorescent labeling (i.e., bimodal imaging) to track proteins, cells, and angiogenesis was recently reported (23–25).

The objective of the present investigation was to document the integration of biodegradable hydrogels implanted s.c. in rats using bimodal fluorescence/MRI imaging and to compare this to the angiogenic effect of VEGF, released from three geometric hydrogel configurations made from the exact same precursor constituents: preformed 5-mm cylindrical plugs, preformed injectable spherical microbeads (200–500 μm), and in situ polymerized injectable hydrogels. The in vivo degradation of these three hydrogel configurations was monitored by MRI, and implant volume was measured and compared. In addition, the fluorescence signal was documented using an IVIS200 system, providing release and resorption profiles of degradation products for each of the implantation strategies. The angiogenesis (capillary density and size) triggered by VEGF-loaded PEG-fibrinogen (PF) was estimated and compared with the control. The effect of the degree of cross-linking on the VEGF release and hydrogel degradation kinetics was also determined. Based on the in vitro data, the bimodal imaging, and the immunohistochemical results, we demonstrate that using different implantation strategies can have a significant effect on the implant integration and localized potency of growth factor delivery, and thus should be a major consideration when designing tissue-engineered constructs and delivery systems.

Results and Discussion

MRI Analysis of Hydrogel Integration. PF precursor solution (14) was labeled with gadolinium (Gd) and Cy5.5 to provide cytocompatible magnetic resonance (MR) and fluorescence contrast, respectively (Figs. S1 and S2). The chemical makeup of the labeled PF hydrogels is illustrated in Fig. S3*A*. Three configurations of bimodal contrast-enhanced implants (i.e., cylindrical plugs, microbeads, and in situ cross-linked hydrogels) with the same initial precursor volume and chemical composition were tested for in vivo integration in a rat s.c. model (Fig. S3*B*). The axial plane-MR images reveal a distinct pattern of in vivo integration that is very much dependent on implant configuration (Fig. 1*A*). Gd provided the necessary contrast between the implants and the surrounding tissues to document the implant volume and location at each time interval of the biodegradation process (Movie S1). All three implant configurations remained localized to the site of the implantation. The in situ polymerized hydrogels showed the fastest integration with the host subcutis and were also rapidly cleared, purportedly by proteolysis, and the microbeads showed an intermediate degradation kinetics, whereas the bulky cylindrical constructs were much slower to degrade. Analysis of implant volume revealed the largest differences in the degradation kinetics at 1 wk postimplantation. The cylindrical plugs lost 37% of their initial volume after 1 wk, whereas microbeads lost 61%, and the in situ polymerized hydrogels were almost fully dissociated (Fig. 1*B*). The cylindrical plugs were still visible 3 wk postimplantation, losing 79% of their volume, whereas the microbeads were almost completely resorbed, with very small remnants comprising 7% of the initial volume. No residual hydrogel was detected by MRI with in situ polymerized PF-GdDTPA-Cy5.5 on the third week of the experiment. These results are consistent with previous studies that use other techniques to document how in vivo fate of biomaterial implants is dependent on the composition, dimensions, in situ environment, and degradation products (13, 15, 26–28). In the

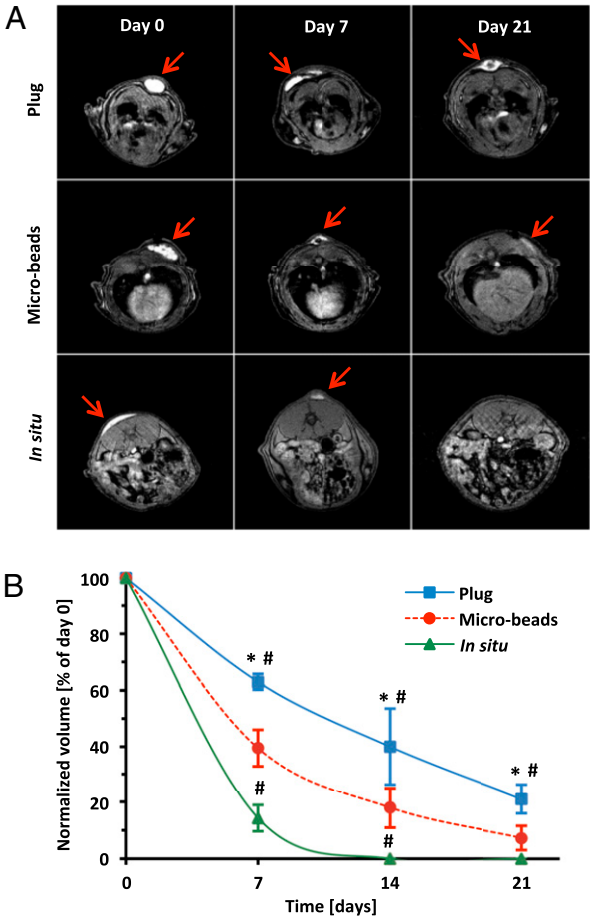

Fig. 1. In vivo MRI analysis of hydrogels. (*A*) Representative axial plane MR images of plugs, microbeads, and in situ polymerized hydrogels. Arrows indicate the Gd-labeled implants. (*B*) Quantitative analysis of the implants' degradation measured as volume reduction at each time point and normalized to day 0. Values are expressed as mean ± SD ($n = 4$–8). $^{*}P < 0.001$ vs. in situ; $^{\#}P < 0.001$ vs. microbeads.

context of hydrogel biomaterial implants specifically, the MRI results are in close agreement with the work of Artzi et al. (15); they also showed that implant geometry significantly affects the in vivo degradation patterns of the implant. Using block and mesh cylinders made with differing surface area-to-volume ratios, they demonstrated that bulky disk-shaped implants were much slower to be resorbed in situ. They also provided evidence that a higher degree of cross-linking limits the rate of in vivo bioresorption. Lower cross-linking efficiency of the in situ polymerized PF hydrogels may also help to explain their disproportionately fast in vivo dissociation in the present study. Specifically, the difficulties in controlling the in situ light-activated cross-linking reaction can result in poor conversion of reactive acrylate groups into cross-links in the PF network, leading to faster resorption kinetics. On the contrary, preformed constructs, such as cylindrical plugs and microbeads, can be cross-linked under controlled conditions, thus ensuring more reliable processing and a more uniform final product (16, 17, 29, 30). Additionally, large preformed constructs have limited access of phagocytic cells and proteolytic enzymes associated with their low surface area-to-volume ratio, resulting in a less efficient in vivo biodegradation, whereas microbeads overcome this limitation by increasing the surface area-to-volume ratio, thus improving accessibility for cells and endogenous proteases.

Fluorescence Analysis of Hydrogel Integration. The fluorescence analysis provided a profile of the degradation products rather than a picture of the intact implant remnants. The degradation products of the PF hydrogels—presumed to be composed of macromolecules of Cy5.5-labeled fibrinopeptides—were initially localized in the regions around the implant locale but became radially diffuse as the hydrogel was reduced in size by the degradation process (Fig. 2*A*). An increase in the maximum fluorescence intensity signal was accompanied by an increase in the total projected area of the signal around the implant locale (Fig. 2*B*). Both these parameters—one representing the amount of degradation product and the other its diffusivity—peaked during the first week and then progressively decreased through day 21. The decrease in total projected area of the signal is likely caused by a dilution of the degradation products as they are cleared from the interstitial space. Interestingly, the rapid increase of fluorescence intensity around the in situ polymerized hydrogels after a few days was much more pronounced compared with the other two treatments (Fig. 2*C*). These data suggest that the in situ polymerized hydrogels dissociate much faster, but the fluorescence intensities (i.e., the amount of degradation product) detected through day 21 suggest that the materials were not necessarily resorbed faster from the implant locale compared with the other hydrogel configurations. The MRI data suggest that the in situ polymerized hydrogels were fully disassembled during the second week in vivo, yet fluorescence data indicate a more sustained bioresorption of the high levels of degradation products from those implants. The microbeads and plugs showed slower degradation based on the MRI data, and sustained bioresorption of fewer degradation products was also evident based on the diminished fluorescence signal through day 21. The integrated fluorescence intensity over the 21 d reveals the highest levels of degradation products for the in situ polymerized injectable treatment, followed by the injectable microbeads, and finally the plugs. Similarly, Phelps et al. (31) demonstrated that fluorescent signal obtained in vivo from labeled VEGF decreased very fast when injected within a soluble PEG hydrogel, demonstrating its fast dissociation and resorption. A more gradual decrease in signal was obtained from prepolymerized degradable PEG hydrogels, and a constant signal was observed in a nondegradable PEG matrix for the same period.

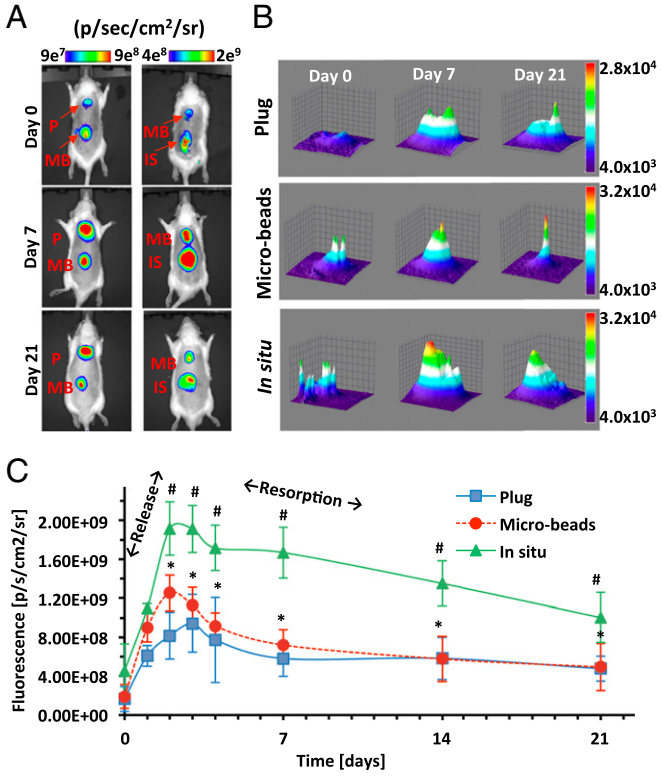

Fig. 2. In vivo fluorescence analysis of hydrogels. (*A*) Whole-animal images of s.c. implanted plugs (P), microbeads (MB), and in situ polymerized (IS) hydrogels. (*B*) Representative 3D plots of the fluorescence signal distribution and intensity. (*C*) Quantitative image analysis of fluorescence signal shows a biphasic temporal pattern of implant degradation and resorption; an initial rise is associated with the rapid release of degradation products from the hydrogel implant, and the subsequent decline is associated with their resorption. Values are expressed as mean ± SD ($n = 2$–7); $^{*}P < 0.01$ vs. in situ; $^{\#}P < 0.0001$ vs. plugs.

Angiogenic Potential of VEGF-Loaded Hydrogels. To evaluate the angiogenic effectiveness of the different configurations, the implant and s.c. tissue samples were stained for the endothelial cell marker CD31 and morphometrically analyzed. Fluorescence images (Fig. 3*A*) and quantitative analysis of the capillary density (Fig. 3*B*) demonstrate that VEGF bolus injections and plugs containing VEGF have relatively low levels of vascularity that are similar to the controls. A nonsignificant twofold enhanced vascularity was apparent in the in situ samples containing VEGF, and a very pronounced 16-fold increase in the vascularity was apparent in the VEGF-loaded microbeads group. Further quantification of the capillary size (Fig. 3*C*) showed that VEGF alone and VEGF combined with the in situ polymerized hydrogel led to a significant decrease in the capillary size (83% and 79% of control values, respectively), whereas all other treatments were similar to the control. Our data are corroborated by the findings of Phelps et al. (31), who demonstrated that degradation of PEG hydrogels containing covalently bound VEGF resulted in an increased vascularization in an s.c. model, with high density of small blood vessels adjacent to the implant. Others have shown that the uncontrolled release of supraphysiological amounts of VEGF leads to an irregular network of small capillaries rather than stimulating the formation of functional and stable capillaries (8, 9, 32, 33). Moreover, newly formed vasculature may disappear after a limited VEGF stimulation, whereas a sustained 10- to 14-d exposure to VEGF resulted in the formation of stable blood vessels (8, 9, 34). This phenomenon may explain the relatively low capillary density and capillary area in the bolus VEGF and in situ groups.

We speculate that the distinct release profile of VEGF from the microbeads was responsible for the potent angiogenic response observed in these samples—this being attributed mostly to their high surface area-to-volume ratio. VEGF is released from fibrinogen materials based on either liberation from the degrading hydrogel and/or passive diffusion (34, 35). With regards to the latter, VEGF has a high affinity to the fibrin and fibrinogen, endowing fibrin-based hydrogels with sustained release for VEGF (35–37). We previously demonstrated that the in vitro release of VEGF from PF plugs was sustained for up to 30 d; the VEGF that was released was biologically active and promoted in vitro proliferation and migration of human aortic endothelial cells (38). Based on this previous work, we can anticipate that the high-affinity VEGF will be released from the hydrogel with the degradation products associated with proteolysis of the implant. Nevertheless, the rapid release of VEGF resulting from differences in the degree of hydrogel cross-linking cannot be discounted in this study, particularly in the case of the in situ polymerized hydrogels, where the cross-linking efficiency may be compromised by the mode of implantation.

Using in vitro characterization, we found a strong inverse correlation between the cross-linking density and the amount of VEGF released from our hydrogels, whereas the degradation rate of the hydrogels was proportional to the cross-linking

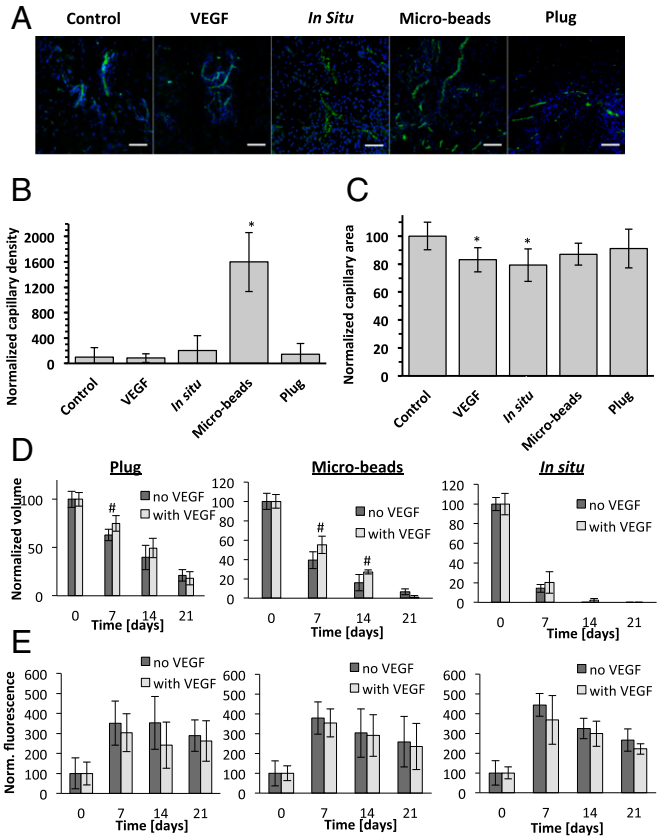

Fig. 3. Immunohistochemical analysis of angiogenesis. (*A*) Representative fluorescent images of tissues stained for CD31 (green) and DAPI (blue). (Scale bars, 50 μm.) (*B*) Capillary density was calculated as number of capillaries per screened tissue area and normalized to the controls. (*C*) Capillary area was measured as total screened capillary area per total capillary number. The effect of VEGF released from three hydrogel configurations on the degradation (*D*) and fluorescent signal intensity (*E*) compared with the unloaded PF hydrogels. Values are expressed as mean ± SD (n = 72–343 screened fields for *B* and *C*; n = 4–8 implants for *D* and *E*); $^{*}P < 0.01$ vs. control; $^{\#}P < 0.05$ vs. untreated hydrogels.

density (Fig. 4). Taken together, our results demonstrate that a higher degree of cross-linking (e.g., preformed plugs and microbeads) results in a slower degradation and VEGF release kinetics, whereas a lower degree of cross-linking (presumably the in situ polymerization treatment) causes faster dissolution of the hydrogels with rapid VEGF release (pseudoindependently of the surface area-to-volume ratio). When comparing preformed plugs and microbeads, which exhibit identical cross-linking but different surface area-to-volume ratios, it is evident that the enhanced angiogenic response is attributed to the high surface area associated with the geometry of the implant. In this context, a higher surface area-to-volume ratio can contribute to a faster degradation rate and a more rapid diffusion-based release of VEGF from the hydrogel implant. In our system, VEGF release and implant biodegradation are coupled, and further studies to identify the exact mechanism by which the microbead geometry attains its proangiogenic potential are still warranted. However, our observations are also consistent with those of Silva and Mooney (7), who demonstrated that the release kinetics of VEGF was strongly dependent on the degradation of hydrogels possessing a similar biodegradation-based release mechanism. Additionally, Moon et al. (39) demonstrated a significant angiogenic response in a mouse cornea model in the matrix metalloproteinase-sensitive degradable hydrogels, whereby degradation of the implants was followed by robust neovascularization in the scaffold implantation site.

Beyond the angiogenic response, the VEGF in the hydrogels also had a significant influence on the rate of implant resorption. Based on MRI data, VEGF caused a significant delay in the degradation kinetics of plugs at day 7 compared with the unloaded hydrogels (25% vs. 37% volume reduction, respectively, Fig. 3*D*). Similar results were observed in the microbeads group, whereby VEGF-loaded microbeads lost 45% of their initial volume at day 7, and 73% at day 14, whereas unloaded microbeads lost 61% and 84%, respectively. This effect was less prominent for the in situ group and for all of the hydrogel groups at day 21. Although the release of the fluorescent marker following the degradation of the hydrogels was not statistically different between the empty PF hydrogels and VEGF-loaded hydrogels, it was reduced in all of the VEGF-treated groups for all time points. This reduction in the fluorescence signal also correlates well with the decrease of the degradation kinetics of the VEGF-loaded hydrogels. The delay in degradation could be attributed to the fact that the biological processes affecting implant resorption in the host are also influenced by the VEGF, including cell–biomaterial interactions and paracrine signaling associated with the implant bioactivity (28, 37, 40, 41). We speculate that the proangiogenic environment induced by the released VEGF at the

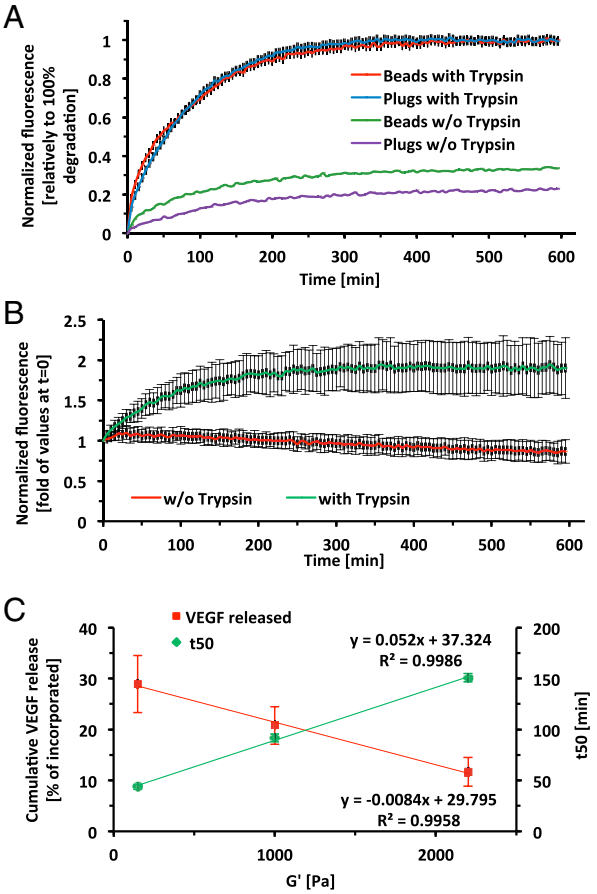

Fig. 4. In vitro characterization of hydrogel degradation and VEGF release as a function of geometry and degree of cross-linking. (*A*) A biodegradation assay was performed on cross-linked PF-Cy5.5 plugs and microbeads in trypsin solution (red and blue, respectively) or in PBS (green and purple, respectively). (*B*) A biodegradation assay was performed on soluble PF-Cy5.5, in samples containing trypsin (green), or without trypsin (red). (*C*) Cumulative VEGF release and in vitro degradation of PF hydrogels with increasing degree of cross-linking. Values are expressed as mean ± SD (n = 3–4).

acute stage of the immune response to the implants (i.e., first week postimplantation) created an environment that would be less accessible to inflammatory cell invasion. This speculation is based on previous findings demonstrating that VEGF exerts strong profibrotic effects in a dose-dependent manner (42, 43). However, the exact link between the inclusion of the proangiogenic factor and the inhibition of hydrogel degradation is still poorly understood and should be further investigated.

Proposed Mechanism of Hydrogel Biointegration. Explanted tissue samples were histologically sectioned and stained with H&E to assess the mechanism of implant resorption and biointegration. The histology of the subcutis at week 3 contained entire segments of intact plug constructs, a few particles from the microbeads, and no evidence of remaining implant in the in situ polymerized samples (Fig. 5, *I* and *II*). Unstained cross-sections were mounted and visualized for Cy5.5 using fluorescence microscopy; the colocalization of Cy5.5 signal with the eosinophilic implant remnants confirms these observations (Fig. 5, *III*). The histological data further reinforced the notion that the implant degradation and resorption were based, at least in part, on phagocytosis. The presence of macrophages was a clear indication that the inflammatory response toward the implanted materials resulted in cell-mediated disassembly and clearance of the hydrogel. Moreover, this mode of degradation is evidenced by the small cavities bordering the interface and inside the implants (Fig. 5, *II*). All three groups exhibited a relatively mild macrophagic reaction, and most of the macrophages were concentrated along the interface of the hydrogel remnants. It is this inflammatory response and hydrogel clearance—usually in combination with the secretion of cytokines and growth factors—that leads to functional tissue regeneration (44–46). These observations were also in agreement with our previous studies using PF plugs in a bone segmental defect model as well as with injectable PF hydrogels in a cardiac myocardial infarction model (47, 48). Our findings thus concur that mode of implantation can play an important role not only in the degradation and resorption properties of the materials, but also in subsequent tissue repair processes. We have also shown that microbeads are a potentially preferable configuration, as they combine the advantages of controllable cross-linking, high surface area-to-volume ratio and injectable mode of implantation.

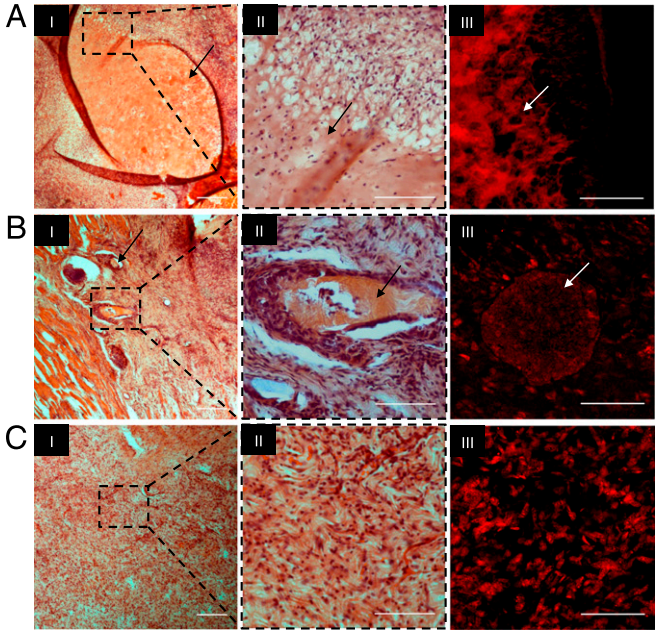

Fig. 5. Histological analysis of s.c. tissue with PF-GdDTPA-Cy5.5 implants. H&E staining of plug constructs (*A*, *I*), microbeads (*B*, *I*), and in situ polymerized implants (*C*, *I*). (Scale bars, 250 μm.) Histopathological evaluation of the selected area with higher magnification revealed no evidence of necrosis or severe inflammation (*A*–*C*, *II*). (*A*–*C*, *III*) Shown are unstained histological sections imaged by fluorescence microscopy for Cy5.5. Arrows indicate remnants of the hydrogel. (Scale bars, 100 μm.)

Advantages of Bimodal Imaging. Bimodal MRI/fluorescence imaging stands to become a powerful research tool in the pursuit of optimized biodegradable materials for tissue regeneration. Even though various methods have been developed to document the fate of biomaterials and to track cellular events in vivo (24, 49–51), none of these has been able to noninvasively monitor the precise dynamics of implant integration. The rate at which a biomaterial is degraded has usually been quantified using in vitro methods (14, 20, 52, 53), which are poorly correlated with in vivo resorption of the material and offer limited insight into the ultimate fate of the implant. Postmortem assessment by histological staining is a common method for determining the resorption of biomaterials; however, terminal assessment at each time point significantly limits the transient resolutions provided by this methodology and significantly increases the number of animals needed for each experiment. In addition, animal killing for terminal evaluations make such methods impractical for eventual clinical use. Marler et al. (54) periodically measured an implanted hydrogel's external volume in a live animal model in an attempt to gain perspective on the transient resorption of the material. However, in vivo degradation and integration of biomaterial implants is a complex process, influenced by a number of factors, and difficult to characterize using a single measurement of implant size. To more effectively predict the in vivo performance of biomaterials using techniques that are quantitative and sufficiently sensitive, we showed that combined MRI and fluorescence imaging are effective as a noninvasive methodology to continuously follow the fate of implanted hydrogel materials with sensitivity and accuracy. A bimodal imaging methodology thus provides the most comprehensive characterization of implant resorption while overcoming many of the most prominent limitations of existing techniques currently in use.

Conclusions

The ability to predict spatial and temporal patterns of biomaterial degradation in vivo is crucial to the design of engineered cell scaffolds and matrices for controlled delivery. For example, when designing a delivery platform for controlled release of bioactive factors and drugs from the polymer, where the liberation of the content is dependent on polymer degradation, hydrogel configuration may serve as a decisive factor. Specifically, the in situ polymerization approach can be used in cases where there is a need for faster and more diffusive release of the bioactive payload. In contrast, for treatments that require a much more sustained bioactivity, one can use bulk constructs as a delivery platform. The use of microbeads could bridge between the very rapid release associated with in situ polymerization and the much more moderate bioactivity of the bulk geometry described herein. As such, microbeads are a preferred platform for the minimally invasive delivery of the bioactive factor VEGF and could be adapted to a variety of other growth factors and biomaterial applications, including cell-seeded scaffolds for tissue engineering and controlled drug delivery systems. Furthermore, the qualitative and quantitative aspects of bimodal imaging described in this study provide important insight into the examination of the in vivo material stability, integration, and resorption as related to the therapeutic potential of an implant material.

Materials and Methods

Fibrinogen PEGylation, labeling, and fabrication of the hydrogel constructs was performed according to published protocols detailed in *SI Materials and*

Methods. Validation of the labeling, biodegradation, VEGF release, and cellular toxicity were performed with in vitro assays using PF containing MRI and fluorescence contrast agents. Subcutaneous implantation, fluorescence imaging, and MRI were performed in a rat model with the approval of the Technion animal care committee. Histological assessment and immunohistochemistry were performed at the terminal time point. Statistical analysis was performed on all quantitative data.

ACKNOWLEDGMENTS. We wish to thank the Preclinical Research Authority and the Imaging and Microscopy Center at the Bruce Rappaport Faculty of Medicine for their help and technical support. This work was supported by the Singapore National Research Foundation (D.S. and A.B.), the Lorry I. Lokey Interdisciplinary Center for Life Sciences and Engineering (D.S.), Russell Berrie Nanotechnology Institute (D.S.), EC-IP FP7 Grants Angioscaff and Biodesign (to D.S.), and in part by the 7th Framework European Research Council Advanced Grant 232640-IMAGO (to M.N.). M.N. is incumbent of the Helen and Morris Mauerberger Chair.

1. Seliktar D (2012) Designing cell-compatible hydrogels for biomedical applications. *Science* 336(6085):1124–1128.
2. Malda J, Klein TJ, Upton Z (2007) The roles of hypoxia in the in vitro engineering of tissues. *Tissue Eng* 13(9):2153–2162.
3. Kellner K, et al. (2002) Determination of oxygen gradients in engineered tissue using a fluorescent sensor. *Biotechnol Bioeng* 80(1):73–83.
4. Bland E, Dréau D, Burg KJ (2013) Overcoming hypoxia to improve tissue-engineering approaches to regenerative medicine. *J Tissue Eng Regen Med* 7(7):505–514.
5. Griffith CK, George SC (2009) The effect of hypoxia on in vitro prevascularization of a thick soft tissue. *Tissue Eng Part A* 15(9):2423–2434.
6. Yancopoulos GD, et al. (2000) Vascular-specific growth factors and blood vessel formation. *Nature* 407(6801):242–248.
7. Silva EA, Mooney DJ (2007) Spatiotemporal control of vascular endothelial growth factor delivery from injectable hydrogels enhances angiogenesis. *J Thromb Haemost* 5(3):590–598.
8. Davies N, et al. (2008) The dosage dependence of VEGF stimulation on scaffold neovascularisation. *Biomaterials* 29(26):3531–3538.
9. Dor Y, et al. (2002) Conditional switching of VEGF provides new insights into adult neovascularization and pro-angiogenic therapy. *EMBO J* 21(8):1939–1947.
10. Seliktar D, Zisch AH, Lutolf MP, Wrana JL, Hubbell JA (2004) MMP-2 sensitive, VEGF-bearing bioactive hydrogels for promotion of vascular healing. *J Biomed Mater Res A* 68(4):704–716.
11. Formiga FR, et al. (2010) Sustained release of VEGF through PLGA microparticles improves vasculogenesis and tissue remodeling in an acute myocardial ischemia-reperfusion model. *J Control Release* 147(1):30–37.
12. Urech L, Bittermann AG, Hubbell JA, Hall H (2005) Mechanical properties, proteolytic degradability and biological modifications affect angiogenic process extension into native and modified fibrin matrices in vitro. *Biomaterials* 26(12):1369–1379.
13. Yilgor P, et al. (2013) An in vivo study on the effect of scaffold geometry and growth factor release on the healing of bone defects. *J Tissue Eng Regen Med* 7(9):687–696.
14. Dikovsky D, Bianco-Peled H, Seliktar D (2006) The effect of structural alterations of PEG-fibrinogen hydrogel scaffolds on 3-D cellular morphology and cellular migration. *Biomaterials* 27(8):1496–1506.
15. Artzi N, et al. (2011) In vivo and in vitro tracking of erosion in biodegradable materials using non-invasive fluorescence imaging. *Nat Mater* 10(9):704–709.
16. Aghion E, Levy G, Ovadia S (2012) In vivo behavior of biodegradable Mg-Nd-Y-Zr-Ca alloy. *J Mater Sci Mater Med* 23(3):805–812.
17. Yang Z, et al. (2012) In vitro and in vivo characterization of silk fibroin/gelatin composite scaffolds for liver tissue engineering. *J Dig Dis* 13(3):168–178.
18. Ge Y, Mei Z, Liu X (2011) Evaluation of daidzein-loaded chitosan microspheres in vivo after intramuscular injection in rats. *Yakugaku Zasshi* 131(12):1807–1812.
19. Cunha-Reis C, El Haj AJ, Yang X, Yang Y (2013) Fluorescent labeling of chitosan for use in non-invasive monitoring of degradation in tissue engineering. *J Tissue Eng Regen Med* 7(1):39–50.
20. Yang Y, Yiu HH, El Haj AJ (2005) On-line fluorescent monitoring of the degradation of polymeric scaffolds for tissue engineering. *Analyst (Lond)* 130(11):1502–1506.
21. Dello SA, et al. (2007) Liver volumetry plug and play: Do it yourself with ImageJ. *World J Surg* 31(11):2215–2221.
22. Zheng J, Allen C, Jaffray D, Chopra A (2004) PEGylated liposome co-encapsulating iohexol and gadoteridol for multimodal CT and MR imaging. *Molecular Imaging and Contrast Agent Database* (National Center for Biotechnology Information, Bethesda).
23. Dafni H, Israely T, Bhujwalla ZM, Benjamin LE, Neeman M (2002) Overexpression of vascular endothelial growth factor 165 drives peritumor interstitial convection and induces lymphatic drain: Magnetic resonance imaging, confocal microscopy, and histological tracking of triple-labeled albumin. *Cancer Res* 62(22):6731–6739.
24. Kotková Z, et al. (2010) Cyclodextrin-based bimodal fluorescence/MRI contrast agents: An efficient approach to cellular imaging. *Chemistry* 16(33):10094–10102.
25. Dafni H, Landsman L, Schechter B, Kohen F, Neeman M (2002) MRI and fluorescence microscopy of the acute vascular response to VEGF165: Vasodilation, hyper-permeability and lymphatic uptake, followed by rapid inactivation of the growth factor. *NMR Biomed* 15(2):120–131.
26. Ji W, et al. (2012) Biocompatibility and degradation characteristics of PLGA-based electrospun nanofibrous scaffolds with nanoapatite incorporation. *Biomaterials* 33(28):6604–6614.
27. Jiang HL, Tang GP, Weng LH, Zhu KJ (2001) In vivo degradation and biocompatibility of a new class of alternate poly(ester-anhydrides) based on aliphatic and aromatic diacids. *J Biomater Sci Polym Ed* 12(12):1281–1292.
28. Chwalek K, et al. (2011) Two-tier hydrogel degradation to boost endothelial cell morphogenesis. *Biomaterials* 32(36):9649–9657.
29. Ghanaati S (2012) Non-cross-linked porcine-based collagen I-III membranes do not require high vascularization rates for their integration within the implantation bed: A paradigm shift. *Acta Biomater* 8(8):3061–3072.
30. Sheridan MH, Shea LD, Peters MC, Mooney DJ (2000) Bioabsorbable polymer scaffolds for tissue engineering capable of sustained growth factor delivery. *J Control Release* 64(1–3):91–102.
31. Phelps EA, Landázuri N, Thulé PM, Taylor WR, García AJ (2010) Bioartificial matrices for therapeutic vascularization. *Proc Natl Acad Sci USA* 107(8):3323–3328.
32. Ozawa CR, et al. (2004) Microenvironmental VEGF concentration, not total dose, determines a threshold between normal and aberrant angiogenesis. *J Clin Invest* 113(4):516–527.
33. Richardson TP, Peters MC, Ennett AB, Mooney DJ (2001) Polymeric system for dual growth factor delivery. *Nat Biotechnol* 19(11):1029–1034.
34. Ehrbar M, et al. (2008) The role of actively released fibrin-conjugated VEGF for VEGF receptor 2 gene activation and the enhancement of angiogenesis. *Biomaterials* 29(11):1720–1729.
35. Wong C, Inman E, Spaethe R, Helgerson S (2003) Fibrin-based biomaterials to deliver human growth factors. *Thromb Haemost* 89(3):573–582.
36. Sahni A, Francis CW (2000) Vascular endothelial growth factor binds to fibrinogen and fibrin and stimulates endothelial cell proliferation. *Blood* 96(12):3772–3778.
37. Ehrbar M, Metters A, Zammaretti P, Hubbell JA, Zisch AH (2005) Endothelial cell proliferation and progenitor maturation by fibrin-bound VEGF variants with differential susceptibilities to local cellular activity. *J Control Release* 101(1-3):93–109.
38. Rufaihah AJ, et al. (2013) Enhanced infarct stabilization and neovascularization mediated by VEGF-loaded PEGylated fibrinogen hydrogel in a rodent myocardial infarction model. *Biomaterials* 34(33):8195–8202.
39. Moon JJ, et al. (2010) Biomimetic hydrogels with pro-angiogenic properties. *Biomaterials* 31(14):3840–3847.
40. Martino MM, Briquez PS, Ranga A, Lutolf MP, Hubbell JA (2013) Heparin-binding domain of fibrin(ogen) binds growth factors and promotes tissue repair when incorporated within a synthetic matrix. *Proc Natl Acad Sci USA* 110(12):4563–4568.
41. Kim CH, Lee JH, Won JH, Cho MK (2011) Mesenchymal stem cells improve wound healing in vivo via early activation of matrix metalloproteinase-9 and vascular endothelial growth factor. *J Korean Med Sci* 26(6):726–733.
42. Maurer B, et al. (2014) Vascular endothelial growth factor aggravates fibrosis and vasculopathy in experimental models of systemic sclerosis. *Ann Rheum Dis* 73(10): 1880–1887.
43. Yoshiji H, et al. (2003) Vascular endothelial growth factor and receptor interaction is a prerequisite for murine hepatic fibrogenesis. *Gut* 52(9):1347–1354.
44. Rappolee DA, Werb Z (1988) Secretory products of phagocytes. *Curr Opin Immunol* 1(1):47–55.
45. Luttikhuizen DT, Harmsen MC, Van Luyn MJ (2006) Cellular and molecular dynamics in the foreign body reaction. *Tissue Eng* 12(7):1955–1970.
46. Anderson JM, Rodriguez A, Chang DT (2008) Foreign body reaction to biomaterials. *Semin Immunol* 20(2):86–100.
47. Habib M, et al. (2011) A combined cell therapy and in-situ tissue-engineering approach for myocardial repair. *Biomaterials* 32(30):7514–7523.
48. Peled E, Boss J, Bejar J, Zinman C, Seliktar D (2007) A novel poly(ethylene glycol)-fibrinogen hydrogel for tibial segmental defect repair in a rat model. *J Biomed Mater Res A* 80(4):874–884.
49. Hoehn M, et al. (2002) Monitoring of implanted stem cell migration in vivo: A highly resolved in vivo magnetic resonance imaging investigation of experimental stroke in rat. *Proc Natl Acad Sci USA* 99(25):16267–16272.
50. Weir C, et al. (2008) Mesenchymal stem cells: Isolation, characterisation and in vivo fluorescent dye tracking. *Heart Lung Circ* 17(5):395–403.
51. Wang Y, et al. (2011) High MR sensitive fluorescent magnetite nanocluster for stem cell tracking in ischemic mouse brain. *Nanomedicine (Lond Print)* 7(6):1009–1019.
52. Gonen-Wadmany M, Goldshmid R, Seliktar D (2011) Biological and mechanical implications of PEGylating proteins into hydrogel biomaterials. *Biomaterials* 32(26): 6025–6033.
53. Lutolf MP, et al. (2003) Synthetic matrix metalloproteinase-sensitive hydrogels for the conduction of tissue regeneration: Engineering cell-invasion characteristics. *Proc Natl Acad Sci USA* 100(9):5413–5418.
54. Marler JJ, et al. (2000) Soft-tissue augmentation with injectable alginate and syngeneic fibroblasts. *Plast Reconstr Surg* 105(6):2049–2058.